A&A 460, 59–66 (2006)
DOI: 10.1051/0004-6361:20065431

Astronomy & Astrophysics

Warm-hot intergalactic medium contribution to baryonic matter

A. M. Sołtan

Nicolaus Copernicus Astronomical Center, Bartycka 18, 00-716 Warsaw, Poland
e-mail: soltan@camk.edu.pl

Received 13 April 2006 / Accepted 10 August 2006

ABSTRACT

Context. Hydrodynamical simulations indicate that a substantial fraction of baryons in the universe remains in a diffuse component – warm-hot intergalactic medium (WHIM).
Aims. The goal of this paper is to determine the physical properties (spatial distribution, temperature, and density) of the WHIM.
Methods. Spatial structure of the soft extended X-ray emission surrounding field galaxies is carefully investigated using the XMM-Newton EPIC/MOS observations. Angular correlations between the galaxy distribution and the soft X-ray background extending over several arcmin result from the large-scale clustering of galaxies. At small angular scales (below ∼2′), the excess of the soft flux is interpreted as the genuine emission from halos of the WHIM surrounding individual galaxies.
Results. Bulk parameters of the average WHIM halos associated with galaxies in the sample are estimated. A typical halo has a characteristic radius of ∼0.3 Mpc and a mass of $3{-}7 \times 10^{11}\ M_{\odot}$. The average density of the WHIM detected in soft X-rays in the local universe, $\rho_{\rm WHIM}$, amounts to $5{-}11 \times 10^{-32}\,{\rm g\,cm^{-3}}$ ($\rho_{\rm WHIM}/\rho_{\rm baryon} = 8{-}19\%$). The range of uncertainties reflects both the statistical scatter of the investigated correlations and our poor knowledge of the WHIM characteristics (e.g., metallicity). It is possible that the actual uncertainties are larger.
Conclusions. Observations of the X-ray WHIM emission are in good agreement with the numerical simulations, but accuracy of the observational material is insufficient to constrain the theory of WHIM. A series of deep observations of a moderately numerous sample of low redshift galaxies with high resolution instruments of *Chandra* would significantly improve our estimates of the WHIM parameters.

Key words. X-rays: diffuse background – intergalactic medium – X-rays: galaxies

1. Introduction

Both theoretical arguments and observational data point out that a major fraction of baryons in the local universe remains in the form of the diffuse component. Galaxies and clusters contribute to the baryonic mass density substantially below the amplitude derived from the primordial nucleosynthesis (e.g., Persic & Salucci 1992; Read & Trentham 2005). Following the first hydrodynamical simulations by Cen & Ostriker (1999), several independent groups (e.g., Davé et al. 2001; Bryan & Voit 2001; Croft et al. 2001) investigated the evolution of the primordial gas distributed outside large concentrations of mass, viz. galaxies and clusters. According to simulations, 30–40% of the baryonic matter has not yet concentrated in gravitationally bound objects. This diffuse component gradually flows toward potential wells created by (mostly) non-baryonic dark matter.

The rate at which the gas flows toward the galaxies depends on the structure of the gravitational potential and the efficiency of the non-gravitational heating, the so-called feedback (e.g., Zhang & Pen 2002). This comprehensive term stands for complex processes associated with the transfer of energy and matter from galaxies back to the intergalactic medium. Although details of these processes are not fully recognized and modeled, basic conclusions drawn from the calculations by all the research groups agree. It is found that the interaction between the infalling gas and the galaxy generates shocks, which heat the intergalactic material. In effect galaxies are surrounded by halos of plasma with temperatures and densities distinctly higher than those in the areas not affected by the feedback.

Simulations predict a wide range of intergalactic plasma temperatures. In the local universe, characteristic temperatures of the model gas accumulating around galaxies increase to $10^5{-}10^7$ K, while in the more remote regions gas remains at the temperatures of $\sim 10^4$ K. The densities of the heated gas also fluctuate and span a wide range of magnitudes. A substantial fraction of baryons is predicted to undergo rather moderate compression with a median overdensity of ∼20 over the cosmic mean (Davé et al. 2001). However, most of the X-ray-emitting gas has densities 100–1000 times greater than the mean (Croft et al. 2001). In this way, the cosmological simulations of the matter evolution indicate that a measurable fraction of baryons constitutes a specific *phase* of matter, the so-called *warm-hot intergalactic medium* (WHIM) (Davé et al. 2001).

A cloud of the WHIM might reveal its existence either through the intrinsic emission of the thermal radiation or through absorption lines induced in spectra of the background objects. Potentially, both effects can be used to evaluate physical parameters of the gas (spatial structure, temperature, density) and eventually to constrain models of the WHIM evolution. Estimates based on the simulations indicate that the expected equivalent width of absorption lines as well as luminosities generated by the individual WHIM clouds are extremely low. Nevertheless, detections of absorption lines produced by the intergalactic hot plasma have been reported by several groups (e.g., Tripp et al. 2000; Nicastro et al. 2005, and references therein). Observations of O^{6+} Kα absorption lines in the spectrum of the blazar MKN 421 by Nicastro et al. (2005) have been used to make a statement on statistical characteristics of the WHIM and its contribution to the local cosmological mass density.

Extragalactic thermal radiation has been searched by Kuntz et al. (2001). These authors investigated the surface brightness of the soft XRB in the *ROSAT* All-Sky Survey (RASS) and detected a smooth thermal component with $kT = 0.23$ keV, which most likely was a mixture of the WHIM and the Galactic halo emission. The existence of gaseous halos of a radius of 30−40 kpc surrounding the spiral galaxy NGC 5746 has recently been reported by Pedersen et al. (2005). The authors argue that the observed halo is formed from the in-flowing gas rather than from the matter expelled in the supernova explosions.

In the present paper we continue our WHIM studies by investigating the soft X-ray emission generated by this phase of the baryonic matter. The main objective of the paper is to determine physical characteristics of the emitting plasma and – eventually – to assess the contribution of the WHIM to the total mean space density of the baryonic matter. In a series of earlier papers we analyzed the structure of the soft X-ray background (XRB). Using the RASS maps we detected soft enhancements of the XRB flux around clusters of galaxies (Sołtan et al. 1996) and galaxies (Sołtan et al. 1997). Assuming a thermal origin of this excess flux, Sołtan et al. (2002) have shown that the temperature of the emission $kT \lesssim 0.5$ keV is in agreement with the expected temperature of the WHIM. We have extended our analysis toward smaller angular (and spacial) scales using the *ROSAT* and XMM-Newton pointing observations and confirmed that the surface brightness of the soft X-ray excess flux increases as the distance to the galaxy diminishes, again as expected for the WHIM structure (Sołtan et al. 2005).

In this paper the spatial properties of the WHIM are investigated in greater detail. Scrupulous analysis of the XRB structure in the XMM-Newton data allowed us to determine the characteristic size and luminosity of the X-rays emitting a WHIM halo around field galaxies. Two fundamental factors complicate observations of the WHIM emission. First, the weak and diffuse WHIM signal is observed against the highly variable background produced by a whole variety of discrete sources. The integral background is dominated by point-like sources identified mostly with all kinds of AGN (e.g., Alexander et al. 2003; Worsley et al. 2005, and references therein), leaving not much space for the diffuse component. To increase the signal-to-noise ratio of the WHIM component, all the detected point sources are removed from the data. Still, the sources below the detection threshold generate fluctuations that impede the WHIM search. Second, due to relatively low temperatures, the thermal emission by the WHIM is expected to be soft, typically below 1 keV, with most of the flux at ∼0.5 keV. At such low energies the absorption of extragalactic photons by the cold gas in the Galaxy is significant, and the search for the WHIM emission has to be limited to high galactic latitudes. In the next section a short description of the observational material used in the analysis is given. The method of calculations and the raw results are presented in Sect. 3. The interpretation of the detected signal is performed in Sects. 4 and 5. A brief discussion is provided in Sect. 6.

2. Observational material

All the simulations of the WHIM emission (e.g., Bryan & Voit 2001; Croft et al. 2001) and our earlier estimates show that the surface brightness of an individual WHIM cloud does not exceed a few percent of the average XRB level. To achieve a meaningful signal-to-noise ratio for the WHIM emission, one requires an extensive set of data. An effective method to measure the weak enhancements of the XRB around galaxies is to calculate the cross-correlation function (CCF) of the XRB and the sample of galaxies. To draw quantitative conclusions from the CCF, one has to remove systematic effects, which could mimic the diffuse signal, from the XRB maps. Also, the sample of galaxies should have well-defined statistical properties.

2.1. EPIC MOS data

In the present analysis the X-ray data are extracted from the public archive[1] of the XMM-Newton EPIC/MOS observations. The pointings are selected in the same way as in the work by Sołtan et al. (2005); for the full description of the data reduction, the reader is referred to Sect. 2.2 of that paper. Here only the main points are recalled and some modifications of the original procedures described.

All the data obtained with the MOS1 and MOS2 detectors in a "Full Frame" mode with the thin filter have been inspected, and only pointings "suitable" for the present investigation have been used. The pointings with a strong source, known extended source, or high particle background have been classified as "unsuitable". To optimize our search of the WHIM signal, new (in comparison to Sołtan et al. 2005) energy bands have been selected: 0.3−0.5 keV, 0.7−1.0 keV, 1.0−1.35 keV, 1.9−3.0 keV, and 3.0−4.5 keV. Energy gaps 0.5−0.7 keV and 1.35−1.9 keV diminish Galactic contribution and the strongest internal fluorescent lines, respectively (Nevalainen et al. 2005).

It was pointed by Pradas & Kerp (2005) that to study faint extended sources such as the WHIM using the XMM-Newton EPIC detectors, "all systematic effects must be well understood and reliable methods to eliminate their contribution have to be developed". In the present approach the WHIM emission is analyzed taking advantage of a large number of available observations. Several hundred pointings had been inspected and above 150 were accepted for further processing. A median exposure time of observation used in the investigation is below 10 ks. It was not possible to investigate instrumental effects reported by Pradas & Kerp (2005) separately for each pointing. However, to account for the possible irregularities of the CCD performance, we have introduced a correction to the procedure described in Sołtan et al. (2005). "A sensitivity map" has been generated separately for the MOS 1 and MOS 2 cameras and for the each of our energy bands. The sensitivity map has been constructed as follows. First, all the point-like sources found in the individual observation have been removed. Then, the counts in the detector coordinates for all the pointings were added. In the same way an "integral" exposure map was created. Finally, the summed count distribution was divided by the exposure map. Since the resultant distribution of count rates in pixels is based on a large number of pointings, fluctuations of the cosmic signal are smoothed out. Thus, spatial variations of the count rates represent the mean inhomogeneities of the detector sensitivity. Although this procedure is unable to deal with the time dependent instrumental effects, it allows for the coherent treatment of a large set of the EPIC MOS observations.

2.2. Galaxy data

The galaxy sample has been extracted from the APM Galaxy Survey (Maddox et al. 1990a,b) using the NASA/IPAC Extragalactic Database (NED). All galaxies with magnitudes between 17 and 20 have been included in the investigation.

[1] XMM-Newton Science Archive:
`http://xmm.vilspa.esa.es/external/xmm_data_acc/xsa/index.shtml`

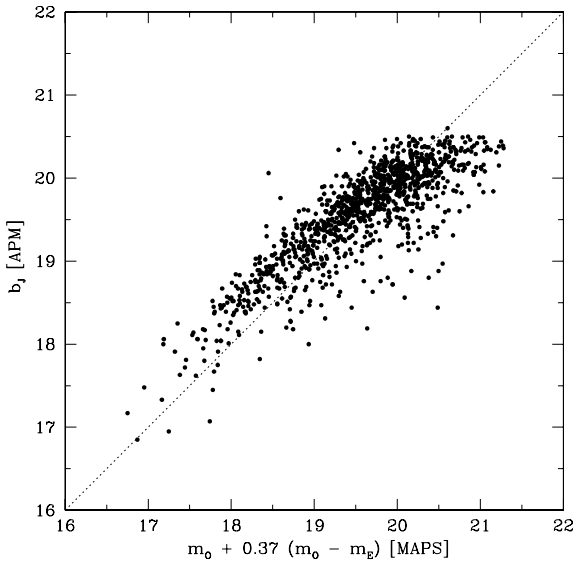

Fig. 1. Comparison of the original b_J magnitudes from the APM Galaxy Survey and the magnitudes derived from m_O and m_E in the MAPS Catalogue.

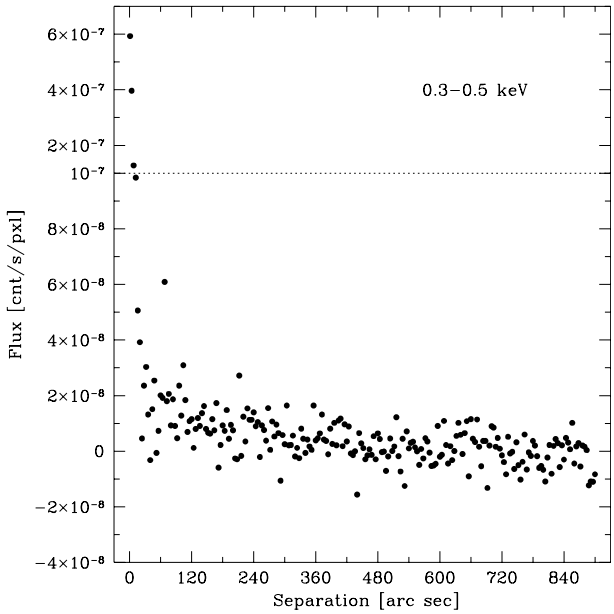

Fig. 2. The count rate distribution in the soft energy band (0.3−0.5 keV) vs. angular distance from the galaxy averaged over the galaxy sample. To display the data points at the smallest separations, the scale at the y-axis above the dotted line has been compressed by a factor of 10.

This magnitude selection criterion is the same as in the subsample of the APM Galaxy Survey discussed by Maddox et al. (1996). The present galaxy sample, drawn from the statistically complete survey and with well-defined magnitude limits, is more homogeneous than the sample used by Sołtan et al. (2005), and some statistical characteristics of the APM galaxies determined by Maddox et al. (1996) are directly applicable to the present investigation (see below).

In the areas not covered by the APM Survey, galaxies extracted from the Minnesota Automated Plate Scanner (MAPS)[2] Catalog of the POSS I have been used. Selection criteria applied to the the MAPS Catalogue have been constructed to generate a sample of objects with statistical characteristics resembling the APM galaxy sample. Using more than 1100 galaxies common to the APM and MAPS samples, a linear transformation between the O and E magnitudes from MAPS and b_J have been found in the form: $b_J = m_O - 0.37(m_O - m_E)$. Figure 1 shows the distribution of magnitudes in both samples. Although the correlation indicated by the dotted line is not perfect, we expect that galaxies selected from the MAPS have clustering properties and a redshift distribution similar to the APM galaxies.

3. Correlation analysis

The average intensity of the XRB at a distance θ from a randomly chosen galaxy is given by the formula:

$$\rho(\theta) = \frac{\sum n_{\rm cnt}}{\sum n_{\rm pxl} \cdot t_{\rm exp}}, \quad (1)$$

where the sums extend over all pointings and all galaxies, $n_{\rm cnt}$ denotes the total number of counts recorded in $n_{\rm pxl}$ pixels separated by the angle θ from the galaxy, and $t_{\rm exp}$ denotes the appropriate exposure time (see Sołtan et al. 2005 for the detailed description). All the data were binned into $4'' \times 4''$ pixels. The total amplitude of the count rate $\rho(\theta)$ obtained from the set of actual observations is a mixture of the cosmic and local X-ray photons as well as charged particles. One should note, however, that any potential systematic variations of the ρ with the separation angle θ could result exclusively from the genuine changes of the average extragalactic XRB flux associated with the galaxy sample. Thus, the data on the absolute level of the contaminating counts are not crucial for the determination of the $\rho(\theta)$ slope.

The flux distribution around galaxies is related to the CCF, $w(\theta)$, in a standard way:

$$w(\theta) = \rho(\theta)/\bar{\rho} - 1, \quad (2)$$

where $\bar{\rho}$ denotes the total average count rate. The average counts $\bar{\rho}$ and consequently the CCF amplitude are affected by the non-cosmic signal.

To isolate the XRB fraction correlated with the galaxy distribution from the total counts and to remove residual instrumental effects in the $\rho(\theta)$ distribution, a large number of random sets of "galaxy" samples have been generated. The average $\rho_{\rm rand}(\theta)$ count rate distribution of the randomized data provides an estimate of the XRB component uncorrelated with the galaxy sample. The difference between both distributions:

$$\delta\rho(\theta) = \rho(\theta) - \rho_{\rm rand}(\theta), \quad (3)$$

which represents the net correlated signal, is shown for the soft (0.3−0.5 keV) and hard (3.0−4.5 keV) energy bands in Figs. 2 and 3, respectively. Note the change of scale at the y-axis above the dotted line in both figures. The distribution of count rates in the hard energy band is noticeably flat at separations above ∼1′, while in the soft band systematic decrease of the flux with the increasing distance is present over a wide range of separations. Although the same effect is visible in Fig. 4 of Sołtan et al. (2005), the distribution of count rates in the soft band (Fig. 2) is shown here as it is now based on the statistically well-defined, complete sample of galaxies. The scatter of points in Fig. 2 is now reduced due to the larger number of galaxies involved in the analysis. Since the $\delta\rho(\theta)$ function is closely related to the average X-ray emission associated with a single galaxy (see below), the statistical completeness of the galaxy sample is crucial for the estimates of the WHIM emission.

[2] The MAPS database is supported by the University of Minnesota, available at `http://aps.umn.edu/`

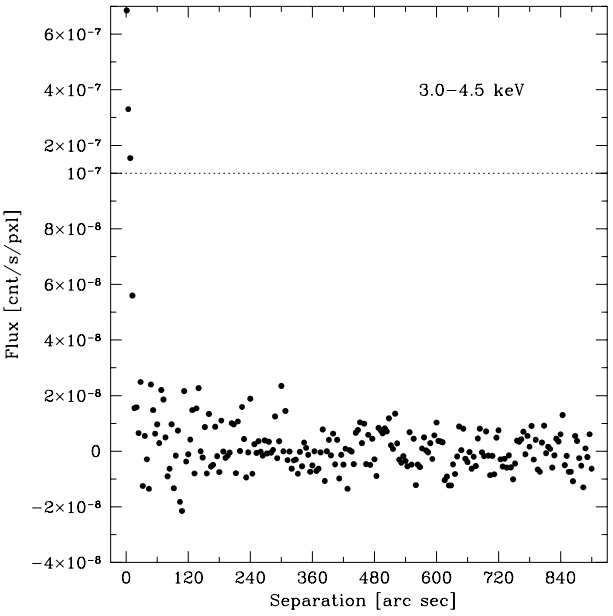

Fig. 3. Same as Fig. 2 in the hard energy band (3.0−4.5 keV).

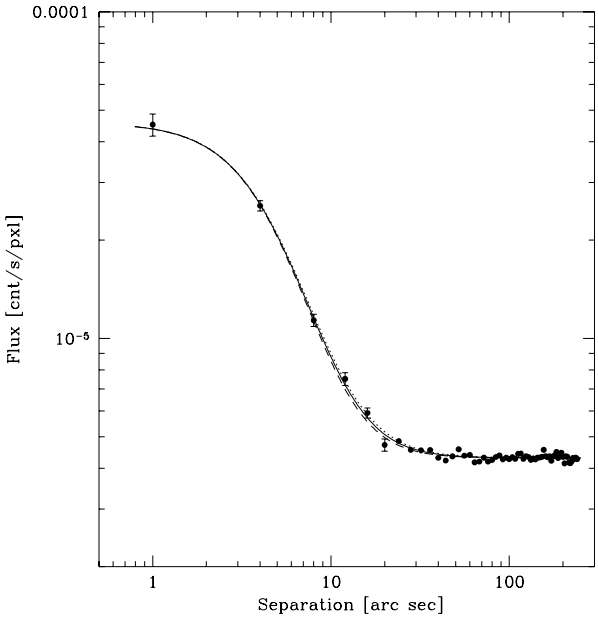

Fig. 4. The count rate distribution in the merged 5 energy bands vs. the distance from a quasar averaged over the distant quasar sample (points with error bars). The curves represent fits of the King profile to the data: solid curve – 5 energy bands merged, dotted curve – 3 soft energy bands merged, dashed curve – 2 hard energy bands merged.

The average surface brightness excess of the XRB around the galaxy is produced by the source(s) "associated" with the galaxy itself and by the nonuniform distribution of neighboring galaxies. So, the integral X-ray emission produced by stellar sources within the galaxy and generated in the extended WHIM halo surrounding the galaxy is defined here as the source "associated" with the galaxy. Let s_i denote the total average flux produced by the galaxy in the ith energy band, $w_{\rm gg}(\theta)$ – the galaxy ACF, and $n_{\rm g}$ – the average concentration of the sample galaxies on the sky. The excess XRB flux above the background level is approximately given by the formula:

$$\delta\rho_i(\theta) \approx s_i \cdot f_i(\theta) + s_i \cdot w_{\rm gg}(\theta) \cdot n_{\rm g}, \quad (4)$$

where the $f_i(\theta)$ function describes the distribution of the galaxy emission in the ith band convolved with the instrument point spread function (PSF). If the WHIM contribution to the $\delta\rho_i(\theta)$ function is negligible and the angular size of the galaxy X-ray emission is much smaller then the width of the PSF, we have:

$$\delta\rho_i(\theta) = s_i \cdot P_i(\theta) + s_i \cdot w_{\rm gg}(\theta) \cdot n_{\rm g}, \quad (5)$$

where $P_i(\theta)$ is the PSF in the ith band. In this case both components of the excess flux at the right hand side of Eq. (5) are easily identified in Fig. 2. A strong peak at small angular separations (below $\sim 1'$) is generated by the point-like galaxy emission, while at larger separations a smooth decrease of the $\rho_i(\theta)$ results from the declining density of neighboring galaxies.

The X-ray emission generated within the galaxy either due to the nuclear activity or in the galactic X-ray sources (X-ray binaries, supernova remnants) is strongly concentrated, and in the present sample of galaxies, the angular extent of the galaxy emission is smaller than the width of the PSF. On the other hand, the genuine emission produced by the WHIM surrounding the galaxy at zero lag is expected to be substantially more extended than the width of the PSF. One should note that this component would be difficult to distinguish from the smoothed flux originating in the neighboring galaxies.

3.1. The effective point spread function

Since the correlation flux $\delta\rho_i(\theta)$ is generated by sources scattered over the entire field of view, the corresponding point source signal should be averaged in the same way. It is assumed that a sample of serendipitous quasars with redshifts greater than 0.3 in the investigated pointings generate count rates that mimic the shape of the point sources' contribution to the $\delta\rho_i(\theta)$. The QSOs have been extracted from the NED, and the average count rate distribution around the sample objects has been determined in the same way as for the galaxy sample. The correlation signal for the quasar sample, $\rho_{\rm QSO}(\theta)$, is shown in Fig. 4. The data points representing the count rates summed over all 5 energy bands are adequately approximated by the King function:

$$\rho_{\rm QSO}(\theta) = \rho_0 \cdot \left[1 + \left(\frac{\theta}{\theta_0}\right)^2\right]^{-y} + \rho_b, \quad (6)$$

with four simultaneously fitted parameters ρ_0, θ_0, y, and ρ_b. Although two shape parameters of the PSF, viz. θ_0 and y, depend on the energy, the effect is neglected in the present analysis. This is because the PSF width variations over our energy bands are minute and do not noticeably affect the present calculations. It is demonstrated in Fig. 4, where three sets of the shape parameters are used to fit the observed count rate distribution. The calculations were performed in two steps. First, the shape parameters were determined separately using three soft energy bands, two hard energy bands, and all 5 bands. Then, two remaining parameters, ρ_0 and ρ_b, were fitted to the count rates in all 5 bands. Three functions pictured in Fig. 4 are practically indistinguishable and in the subsequent calculations we use the PSF shape parameters determined using all the bands.

3.2. The surface brightness distribution

At separations comparable to the width of the PSF, i.e., below $\sim 1'$, the count rates generated in the $\delta\rho_i(\theta)$ by the extended

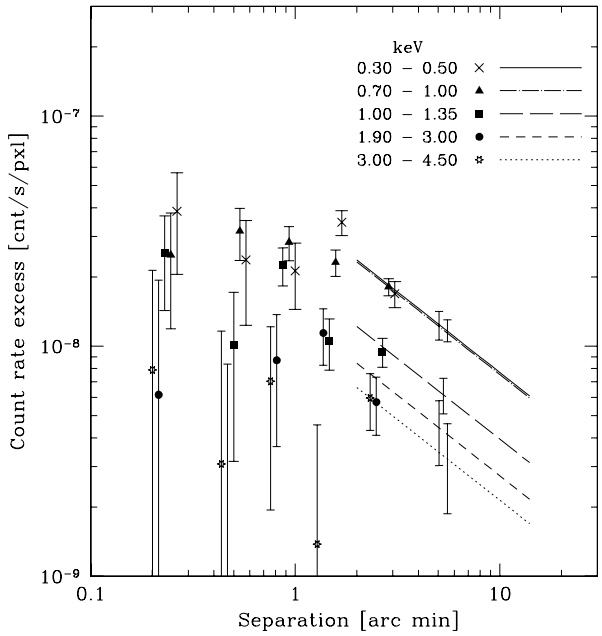

Fig. 5. The average excess count rate distribution around galaxies in five energy bands. For separations above 2′ the power law with a slope of −0.7 is assumed and only the normalization has been fitted to the data. At separations below 2.′7 individual points with the error bars or upper limits are shown. Some points have been slightly displaced for clarity.

emission are superimposed on the relatively strong signal produced by the point-like source identified with the galaxy.

To subtract the point source contribution from the $\delta\rho_i(\theta)$ count rates around galaxies, the PSF has been normalized to the observed distribution at separations below 10″ (first three data points in Fig. 4). The residual flux between 0.″2 and 2.″7 is plotted in Fig. 5. Error bars and upper limits represent statistical uncertainties at 1σ level.

At large angular separation, beyond the WHIM halo surrounding an individual galaxy, enhanced emission results purely from the clustering of galaxies. According to Eq. (4), the amplitude of the correlated signal is defined by the galaxy ACF. Although the angular extension of a typical halo around the galaxy from the sample is a priori unknown, simulations indicate that the WHIM signal is negligible at separations above a few arcmin (e.g., Bryan & Voit 2001; Croft et al. 2001). Consequently, we tentatively assume that the amplitude of $\delta\rho_i(\theta)$ above 2′ is dominated by the galaxy correlation term. The ACF of the APM galaxies has been determined by Maddox et al. (1996):

$$w_{\rm gg}(\theta) = w_0 \cdot \theta^{-0.7}, \tag{7}$$

where $w_0 = 0.50$ for θ in arcmin. Thus, within the framework of the present model, the count rate distributions $\delta\rho_i(\theta)$ at separations greater than 2′ has been approximated by the power law:

$$\delta\rho_i(\theta) = A_i \cdot \theta^{-0.7}, \tag{8}$$

where the amplitude of the correlation signal is related to the average integral flux associated with the galaxy:

$$A_i = s_i\, w_0\, n_{\rm g}. \tag{9}$$

The parameters A_i for 5 energy bands have been fitted to the observational data points for separations between 2′ and 14′, and the best power law fits are shown in Fig. 5. The error bars indicate 1σ uncertainties of the A_i estimates generated only by statistical noise. Because the $\delta\rho_i(\theta)$ functions are based on a large number of pointings, the scatter of points discernible in Figs. 2 and 3 is adequately described by the Poisson statistics of the number of counts contributing to each data point.

Table 1. X-ray fluxes correlated with galaxies.

i	Energy	s_i [10^{-5} cnt/s]		
	[keV]	Total	Point	Extended
1	0.30–0.50	18.3 ± 2.6	1.15	17.2
2	0.70–1.00	18.3 ± 2.0	1.41	16.9
3	1.00–1.35	9.4 ± 1.7	0.92	8.5
4	1.90–3.00	6.5 ± 2.1	0.77	5.8
5	3.00–4.50	5.1 ± 2.2	0.82	4.3

4. The WHIM structure

The total fluxes correlated with the individual galaxy in 5 bands have been determined using Eq. (9) and are given in Table 1. The average density of the APM galaxies in the magnitude range of $17 < b_{\rm J} < 20$ $n_{\rm g} = 0.0944\,{\rm arcmin}^{-2}$ was taken from paper on the APM galaxy counts by Maddox et al. (1996). In the present model, flux per individual galaxy s_i has been split into point-like and extended components. The average flux contained in the point source has been estimated by fitting the PSF to the $\delta\rho_i(\theta)$ at separations below 10″ (i.e., the first three points in the $\delta\rho_1(\theta)$ distribution). The integrated flux of the extended component was obtained by subtraction of the point source from the integral signal. Both components of the correlated flux are given in Cols. 4 and 5 of Table 1. Although, the point-like source is conspicuous in the correlation distribution, $\delta\rho_i(\theta)$, the data in Table 1 show that on the average the extended source is substantially stronger than the point-like source.

One should note that in all the energy bands, the detected fluxes ascribed to the individual galaxy are extremely small. With the mean exposure time for a single pointing of ∼13 ks, the total average signal per galaxy in the soft bands exceeds just two counts, while the point source amounts to a small fraction of one count. Thus, the investigated effects are absolutely below the detection threshold for a single observation, and to achieve a reasonable S/N ratio, the investigation necessarily had to be based on a very extensive data.

Since the galaxy ACF has a roughly constant slope of −0.7 down to at least 0.′3 (Maddox et al. 1996), the substantial flattening of the $\delta\rho_i(\theta)$ distribution below ∼2′ apparent in Fig. 5 indicates that a dominant fraction of the correlated flux is generated indeed in the extended source. Large uncertainties involved in the present analysis and visualized by the error bars in Fig. 5 limit our analysis to the semi-quantitative, gross estimates of the WHIM parameters. In the subsequent calculations, we make assumptions that inevitably introduce simplifications into the WHIM modeling. Albeit some assumptions cannot be verified, the present data do not allow for a more detailed description.

In particular, the WHIM distribution below 2′−3′ is approximated by a well-defined, smooth halo centered on a galaxy. Consequently, the average surface brightness of the WHIM emission is equal to the amplitude of the $\delta\rho_i(\theta)$. Such interpretation of the observations is favored by the maps of the soft X-ray emission based on hydrodynamic simulations by Croft et al. (2001), where the patches of the highest X-ray surface brightness form regular circular areas centered on galaxies. Accordingly,

the mean angular extent of the WHIM halo, $\theta_{\rm halo}$, is estimated using the relationship:

$$\int_0^{\theta_{\rm halo}} 2\,\pi\,\theta\,\delta\rho_i(\theta)\,{\rm d}\theta = s_i^{\rm ext}, \tag{10}$$

where $\delta\rho_i(\theta)$ is the excess count rate distribution after the removal of the central peak produced by the point-like component and $s_i^{\rm ext}$ denotes the flux of the extended source. In rough agreement with Fig. 5, we assume that for the small separations, the excess count rate $\delta\rho_i(\theta)$ is flat and in the energy band 0.3–0.5 keV, $\delta\rho_1(\theta) \approx 3\times10^{-8}\,{\rm cnt\,s^{-1}\,cm^{-2}}$. Substituting the relevant quantities into Eq. (10), the implied mean halo radius $\theta_{\rm halo} = 2\farcm8$. Because of the multi-step procedure involved in the calculation, the formal error estimates of $\theta_{\rm halo}$ are difficult to assess. It is likely that our "best estimate" of the $\delta\rho_i(\theta)$ amplitude at large separations has been overestimated due to some contribution of the individual halo to the power law section of the distribution. The lower value of $s_i^{\rm ext}$ would imply a smaller size of the halo. In our opinion, a realistic estimates of X-ray emitting halo size are between $2'$ and $2\farcm8$. Calculations of the baryonic mass of the halo described in Sect. 5 below account for this uncertainty.

4.1. Temperature of the WHIM

Count rates of the extended source listed in the last column of Table 1 have been used to estimate the mean temperature of the WHIM emission. We applied the following procedure. First, a grid of thermal plasma emission spectra based on the Raymond & Smith (1977) code was generated for a wide range of temperatures and metal abundances. The MIDAS/EXSAS software was used. The spectra were calculated for redshift $z = 0.12$ (see below) and subject to the low energy absorption by cold gas in the Galaxy with the hydrogen column density of $2.2\times10^{20}\,{\rm cm^{-2}}$ (the average value in the sample).

Next, the spectra were convolved with the effective area of the X-ray telescope/EPIC MOS detector system, and the model counts in five energy bands were compared with the data. The best fit with $\chi^2 = 10.1$ for 3 dof was obtained for $kT = 0.50\,{\rm keV}$ and unrealistically low metal abundances relative to the "cosmic abundances" $\zeta = Z/Z_{\rm cosmic} = 0.01$. We conclude that the observed counts are inconsistent with a single temperature model; the distribution of count rates in 5 energy bands is too wide to be fitted by a simple thermal spectrum.

The presence of cluster galaxies in our sample provides a natural explanation of the discrepancy between the data and the single temperature model. Although, our galaxy sample has been carefully examined from the point of view of the cluster contamination and all the known clusters have been removed both from the galaxy sample and the X-ray maps, it is evident that this procedure is not effective in the elimination of all the clusters in the investigated area. In particular, our data unavoidably include some unspecified number of X-ray clusters with the brightest galaxies above the faint magnitude limit of $m_{\rm b} = 20$. Since the sensitivity of the present investigation is very high, even a moderate contamination of the galaxy sample with cluster members could introduce the measurable signal in all the energy bands.

To subtract the contribution of the serendipitous clusters to the extended emission, a thermal spectrum with $kT = 5\,{\rm keV}$ and metal abundances $\zeta = 0.20$ has been adjusted to two hard energy bands (1.9–3.0 and 3.0–4.5 keV). Then, the cluster spectrum was subtracted from the remaining 3 soft energy bands and the fitting procedure to the residual count rates was repeated. Obviously, the temperatures of the new fits were substantially lower than those obtained for the original data. Fits with acceptable χ^2 were obtained for temperatures in the range 0.20–0.30 keV with rather weak constraints on the metallicity. For temperatures close to $kT = 0.20\,{\rm keV}$ high metallicities are favored, while for $kT \gtrapprox 0.25$ low metallicities $\zeta \lessapprox 0.30$ give acceptable fits.

5. Baryon densities

Our estimates of the size and temperature of the average halo are now used to assess the characteristic densities and the total baryonic mass of the WHIM. In the calculations we assume that plasma fills the spherical halo with constant density and the temperature $kT = 0.25\,{\rm keV}$. As indicated in Sect. 4, the halo radii of $2'$ and $2\farcm8$ are considered.

Roughly 80% of the APM galaxies in the magnitude range $17 \le b_{\rm J} \le 20$ have redshifts between 0.06 and 0.22 with the median of the distribution $z_{\rm med} = 0.12$. (Maddox et al. 1996). Luminosity and angular diameter distances defined by this redshift are $D_L = 560\,{\rm Mpc}$ and $D_A = 447\,{\rm Mpc}$, respectively; angular size $\theta_{\rm halo} = 2'$ corresponds to the radius $r_{\rm WHIM} = 260\,{\rm kpc} = 8.0\times10^{23}\,{\rm cm}$ ($H_0 = 70\,{\rm km\,s^{-1}Mpc^{-1}}$, $\Omega_m = 0.3$, and $\Omega_\Lambda = 0.7$ are assumed throughout the paper). We now substitute the results obtained in the paper and all the relevant data into standard formulae:

$$V_{\rm halo} = \frac{4}{3}\,\pi\,r_{\rm halo}^3, \tag{11}$$

$$L_{\rm halo} = V_{\rm halo}\cdot j_E(T), \tag{12}$$

$$L_{\rm halo} = 4\,\pi\,D_L^2\cdot S_{\rm halo}, \tag{13}$$

where $V_{\rm halo}$, $L_{\rm halo}$, and $S_{\rm halo}$ denote respectively: the halo volume, the luminosity, and the corresponding flux at distance D_L from the halo; $j_E(T)$ is the volume emissivity of plasma at energy E and temperature T. Due to the weak constraints on the metallicity of the WHIM (although low metallicities are favored both by simulations and our results) we consider two models of the plasma emission: pure thermal Bremsstrahlung and the thermal plasma with $\zeta = 0.10$. Using the basic formulae for the thermal Bremsstrahlung (e.g., Rybicki & Lightman 1985), for $kT = 0.25\,{\rm keV}$ in the 0.3–0.5 keV energy band, we get:

$$j_E(T) = 6.38\times10^{-25}\,n_p^2\,\frac{\rm erg}{\rm s\,cm^3}, \tag{14}$$

where n_p is the hydrogen density in ${\rm cm^{-3}}$. Equation (14) is valid for the zero metallicity plasma with $Y = 0.25$. For the plasma emission we apply the analogous formula:

$$j_E(T) = 1.32\times10^{-24}\,n_p^2\,\frac{\rm erg}{\rm s\,cm^3}, \tag{15}$$

which is derived for the Raymond & Smith (1977) model using the MIDAS/EXSAS software. Higher plasma emissivity results from metal lines contributing strongly to the total signal at these temperatures. Finally, the count rate $s_1^{\rm ext} = 17.2\,{\rm cnt/s}$ is expressed in the cgs units using the conversion factor of $1\,{\rm cnt} = 0.65\times10^{-11}\,{\rm erg/cm^2}$ calculated for the thermal spectrum with the $kT = 0.25\,{\rm keV}$. Combining all the numerical data, we get the plasma density in the WHIM halo, $\rho_{\rm halo}$, and the baryonic halo mass, $M_{\rm halo}$, for the range of the halo sizes and two emission models. Our results are collected in Table 2.

Table 2. The WHIM halo parameters.

$\theta_{\rm halo}$		Thermal Bremsstrahlung				Plasma emission			
		n_p	$\rho_{\rm halo}$	$M_{\rm halo}$	$\rho_{\rm WHIM}$	n_p	$\rho_{\rm halo}$	$M_{\rm halo}$	$\rho_{\rm WHIM}$
(arcmin)	(cm)	($\rm cm^{-3}$)	($\rm g\ cm^{-3}$)	($M_\odot$)	($\rm g\ cm^{-3}$)	($\rm cm^{-3}$)	($\rm g\ cm^{-3}$)	($M_\odot$)	($\rm g\ cm^{-3}$)
2.0	8.0×10^{23}	1.7×10^{-4}	3.9×10^{-28}	4.2×10^{11}	6.8×10^{-32}	1.2×10^{-4}	2.7×10^{-28}	2.9×10^{11}	4.7×10^{-32}
2.8	1.1×10^{24}	1.1×10^{-4}	2.3×10^{-28}	6.9×10^{11}	1.1×10^{-31}	7.3×10^{-5}	1.6×10^{-28}	4.8×10^{11}	7.8×10^{-32}

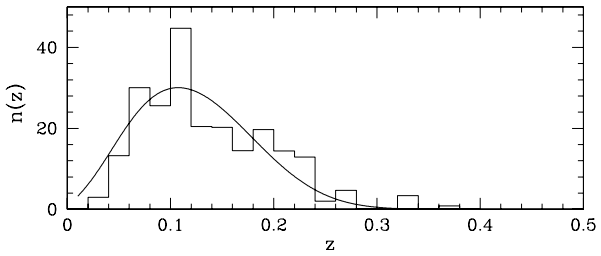

Fig. 6. The model redshift distribution for galaxies in the magnitude range $17 < b_{\rm J} < 20$ derived using the luminosity function given by Folkes et al. (1999). The distribution has been normalized to the histogram of 230 galaxies presented by Maddox et al. (1996).

5.1. WHIM contribution to $\Omega_{\rm baryon}$

Within the framework of the present model, the WHIM contribution to the $\Omega_{\rm baryon}$ is defined by the space density of the WHIM halos centered at galaxies. Because of a large radial density gradient, our magnitude limited sample of galaxies is not well-suited for such estimates. To correct for this effect, the mean spatial density of galaxies contributing to the observed $\delta\rho_i(\theta)$ distribution averaged over redshift should be weighted by the number of galaxies in the sample. Let $n(z)$ denote the average number of galaxies in the magnitude range $17 < b_{\rm J} < 20$ as a function of redshift. The effective spatial density $\langle N\rangle$ of galaxies in the sample is given by the formula:

$$\langle N\rangle = \frac{\int N(z)\cdot n(z)\,{\rm d}z}{\int n(z)\,{\rm d}z}, \qquad (16)$$

where $N(z)$ is the number of galaxies in $1\,{\rm Mpc}^{-3}$ at redshift z within the apparent magnitude range $17 < b_{\rm J} < 20$. Using the luminosity function of galaxies by Folkes et al. (1999) adapted to $H_0 = 70\,{\rm km\,s^{-1}Mpc^{-1}}$, we have determined both the redshift distributions expected in the APM sample, $N(z)$ and $n(z)$. The latter one is shown in Fig. 6, superimposed on the observed histogram of 230 galaxies in the magnitude range $17 < b_{\rm J} < 20$ as given by Maddox et al. (1996). After substitution of these distributions into Eq. (16), we finally got $\langle N\rangle = 2.4\times10^{-3}\,{\rm Mpc}^{-3}$. The average WHIM density $\rho_{\rm WHIM} = M_{\rm halo}\times\langle N\rangle$ and the numerical values of the $\rho_{\rm WHIM}$ are given in Table 2 for all the combinations of the models.

We compare our $\rho_{\rm WHIM}$ estimates with the total baryon content. Assuming the current baryon density $\rho_{\rm baryon} = 0.044\,\rho_{\rm cr} = 4.2\times10^{-31}\,{\rm g\,cm^{-3}}$ (Spergel et al. 2003), the baryon density at the redshift $z = 0.12$ amounts to $\rho_{\rm baryon}(z = 0.12) = 5.9\times10^{-31}\ {\rm g\,cm^{-3}}$. Consequently, the WHIM detected in the soft X-rays at that redshift contributes 8–19% to the baryon density, or $\Omega_{\rm WHIM} = 0.4$–0.8%.

6. Discussion

The present investigation concentrates on two objectives. First, we demonstrate an existence of the extended soft emission correlated with galaxies, which in a natural way is identified with the thermal emission of the WHIM. Second, using the estimates of the X-ray flux correlated with galaxies, we determine the physical parameters of the WHIM: the temperature, the plasma density, and the total mass of the emitting clouds. Very low amplitude of the extended emission superimposed on the granular XRB generated by discrete sources makes the analysis difficult and sensitive to the cosmic and instrumental effects.

The first objective was achieved by the careful evaluation and extraction of several interfering signals and by using extensive observational material. The cross-correlation technique appears to be a highly effective tool in the present analysis. This is because it integrates the delicate X-ray glow surrounding galaxies and efficiently eliminates various intruding signals. The large number of pointings and galaxies reduced the fluctuations virtually to the Poissonian limit defined by the number of galaxy–X-ray count pairs. Our estimates of the amplitude of the extended emission in 5 energy bands have been obtained under the assumption that the WHIM distribution is correlated with galaxies, without any further constraints. Strong correlation between the WHIM and the galaxy distribution is indicated by all the hydrodynamical simulations (e.g., Davé et al. 2001; Bryan & Voit 2001; Croft et al. 2001).

Detailed physical characteristics of the WHIM determined in the paper are not free from assumptions which – albeit plausible – could not be verified by the observations. Most of our estimates of the plasma parameters have been obtained under the assumption that the typical WHIM cloud has a spherical shape. The two-point correlation function gives the WHIM signal averaged over the azimuthal angle. Thus, the method is unable to identify filaments. Although most simulations predict that the WHIM distribution exhibits filamentary structure, it is likely that the spherical symmetry approximation describes the WHIM emission satisfactorily. This is because the elongated structures "visible" in the WHIM simulations have extremely low density and surface brightness, while the regions with high surface brightness are roughly circular. This effect is visualized in Fig. 1 in Bryan & Voit (2001) and Figs. 3 and 5 in Croft et al. (2001).

In the calculations of the halo mass, we assumed smooth and uniform distribution of the gas within a sphere surrounding the galaxy. Such an approximation makes our calculations possible, but it certainly constitutes a simplification to the actual halo structure. Nevertheless, simulations provide some justification for our approach. A qualitative inspection of the diffuse emission maps generated by Croft et al. (2001) reveals surprisingly simple structure at scales typical for the individual halo. Apparently the simulated structures seem to be fairly well modeled in the present paper. Although "visual agreement" between the maps and the simple halo model of the WHIM supports our calculations, the range of the parameter uncertainties of the single halo is probably wider than that formally assessed in the paper. Consequently, our estimate of the average WHIM density is also subject to higher uncertainties. A long chain of calculations

constrained by the series of assumptions makes our error estimates disputable. On the other hand, our best estimates of some parameters (i.e., the plasma temperature and density, the contribution of the WHIM to the total baryon density) fit the corresponding quantities obtained in the hydrodynamical simulations well.

One should note that to constrain the simulations, we need substantially more accurate observational material. It is doubtful that the WHIM emission at separations above several arcmin from the galaxy could be measured with substantially better precision using the present day instruments. However, at smaller separations, below $2'-3'$, where the WHIM surface brightness amounts to several percent of the total soft XRB, a new deep observation of a moderately numerous sample of galaxies at low redshifts would significantly improve our data. Also, at separations of several arcsec, one could take advantage of the superb angular resolution of the *Chandra X-Ray Observatory* and measure the WHIM emission in the immediate vicinity of the galaxies.

Acknowledgements. We thank all the people involved in the XMM-Newton project for making the XMM Science Archive and Standard Analysis System such user-friendly environments. This research has made use of the NASA/IPAC Extragalactic Database (NED), which is operated by the Jet Propulsion Laboratory, California Institute of Technology, under contract with the National Aeronautics and Space Administration. This research has also made use of the MAPS Catalog of POSS I supported by the University of Minnesota. This work has been partially supported by the Polish KBN grant 1 P03D 003 27.

References

Alexander, D. M., Bauer, F. E., Brandt, W. N., et al. 2003, AJ, 126, 539
Bryan, G. L. & Voit, G. M. 2001, ApJ, 556, 590
Cen, R. & Ostriker, J. P. 1999, ApJ, 514, 1
Croft, R. A. C., Di Matteo, T., Davé, R., et al. 2001, ApJ, 557,67
Davé, R., Cen, R., Ostriker, J. P., et al. 2001, ApJ, 552, 473
Folkes, S., Ronen, S., Price, I., et al. 1999, MNRAS, 308, 459
Kuntz, K. D., Snowden, S. L., & Mushotzky, R.F. 2001, ApJ, 548, L119
Maddox, S. J., Sutherland, W. J., Efstathiou, G., & Loveday, J. 1990a, MNRAS, 243, 692
Maddox, S. J., Efstathiou, G., & Sutherland, W. J. 1990b, MNRAS, 246, 433
Maddox, S. J., Efstathiou, G., & Sutherland, W. J. 1996, MNRAS, 283, 1227
Nevalainen, J., Markevitch, M., and Lumb, D. 2005, ApJ, 629, 172
Nicastro, F., Mathur, S., Elvis, M., et al. 2005, Nature, 433, 495
Pedersen, K., Rasmussen, J., Sommer-Larsen, J., et al. 2005, [arXiv:astro/ph/0511682]
Persic, M., & Salucci, P. 1992, MNRAS, 258, 14
Pradas, J., & Kerp. 2005, A&A, 443, 721
Raymond, J. C., & Smith, B. W. 1977, ApJS, 35, 419
Read, J. I., & Trentham, N. 2005, Phil. Trans. Royal Soc., 363, 2693
Rybicki, G. B., & Lightman, A. P. 1985, Radiative Processes in Astrophysics. (New York: A Wiley-Interscience Publication)
Sołtan A. M., Hasinger G., Egger, R., Snowden, S., & Trümper, J. 1996, A&A, 305, 17
Sołtan A. M., Hasinger G., Egger, R., Snowden, S., & Trümper, J. 1997, A&A, 320, 705
Sołtan A. M., Freyberg, M., & Hasinger G. 2002, A&A, 395, 475
Sołtan A. M., Freyberg, M., & Hasinger G. 2005, A&A, 436, 67
Spergel, D. N., Verde, L., Peiris, H. V., et al. 2003, ApJ 148, 175
Tripp, T., Savage, B., & Jenkins, E. 2000, ApJ, 534, L1
Worsley, M. A., Fabian, A. C., Baure, F. E., et al. 2005, MNRAS, 357 1281
Zhang, P. J., & Pen, U. L. 2002, ApJ, 588, 704